materials

MDPI

Article

Effect of Service Environmental Parameters on Electrochemical Corrosion Behavior of L80 Casing Steel

Xiaoguang Sun [1,2], Huaiyun Cui [1], Zhong Li [3,4], Renyang He [5], Zhiyong Liu [1,*] and Lin Lu [1,*]

1 Institute for Advanced Materials and Technology, University of Science and Technology Beijing, Beijing 100083, China; sunx_sf@126.com (X.S.); cuihuaiyun@163.com (H.C.)
2 CRRC Qingdao Sifang Co., Ltd., Qingdao 266111, China
3 Chinese Society for Corrosion and Protection, Beijing 100083, China; zl129616@ohio.edu
4 Department of Chemical and Biomolecular Engineering, Institute for Corrosion and Multiphase Technology, Ohio University, Athens, OH 45701, USA
5 China Special Equipment Inspection and Research Institute, Beijing 100029, China; herenyang@163.com
* Correspondence: liuzhiyong7804@126.com (Z.L.); lulin315@126.com (L.L.)

Abstract: The corrosion behavior of L80 casing steel was studied in a simulating annulus environment using the electrochemical measurement method, immersion test, and tensile test under a high-temperature and high-pressure H_2S/CO_2 environment. The partial pressure of CO_2 (P_{CO_2}), the partial pressure of H_2S (P_{H_2S}), water content, and preloading stress remarkably affected the corrosion behavior of L80 steel. The influence of P_{CO_2} on stress corrosion cracking (SCC) susceptibility has an inflection point of approximately 1.1 MPa. The SCC susceptibility reaches the maximum when the P_{CO_2} is about 1.1 MPa. The SCC susceptibility has a positive correlation to P_{H_2S} and water content. The higher water content of the corrosion medium can increase the electrical conductivity of the corrosion medium and promote the corrosion of L80 steel, which can improve the diffusion of hydrogen into steel and promote the SCC of L80 steel. Preloading stress can promote local corrosion, thereby promoting SCC of steel under stress. The dislocation emergence point caused by preloading stress can accelerate the diffusion of hydrogen into steel and increase SCC susceptibility.

Keywords: L80 casing steel; annulus environment parameters; stress corrosion; electrochemical; preloading stress

Citation: Sun, X.; Cui, H.; Li, Z.; He, R.; Liu, Z.; Lu, L. Effect of Service Environmental Parameters on Electrochemical Corrosion Behavior of L80 Casing Steel. *Materials* **2021**, *14*, 5575. https://doi.org/10.3390/ma14195575

Academic Editors: X. Ramón Nóvoa and Frank Czerwinski

Received: 24 July 2021
Accepted: 10 September 2021
Published: 25 September 2021

1. Introduction

During oil and gas exploitation, CO_2 and H_2S, as associated media, cause serious corrosion damage to oil and gas production equipment, thereby restricting the exploitation of oil and gas fields [1–3]. CO_2 and H_2S are important influential parameters for oil and gas equipment corrosion. CO_2 primarily causes electrochemical corrosion, which leads to local pitting corrosion and perforation damage of materials [4,5]. Some researchers have also reported that CO_2 can cause stress corrosion when dissolved in water [6,7]. On the contrary, H_2S is more harmful to equipment. H_2S can cause hydrogen-induced cracking and sulfide stress corrosion cracking, which lead to the breakdown of equipment and can cause huge economic losses and heavy casualties [8–11].

A huge amount of H_2S and CO_2 is found in the annulus environment because of carbonate, sulphate-reducing bacteria, high temperature, high pressure, and other factors [12,13]. In this environment, serious accidents such as leakage and the fracture of casing steel often occur, which leads to the scrapping of the whole oil well [14–16]. Casing is the key structure that supports the structural stability and safety of an oil well, and its integrity determines its lifespan. Controlling stress corrosion is important to maintain the safe and stable production of oil wells [4,17]. In the annulus of an oil well, some oil films and scale layers are found on the surface of casing steel because of the presence of mineralized water and a small amount of infiltrated crude oil, which slows down the uniform

corrosion to a certain extent [18–20]. Therefore, the corrosion of downhole tubes is due to corrosion perforation and stress corrosion fracture under the scale. This case signifies that the sensitivity of stress corrosion of downhole tubes in the annular environment of a production well may be lower than that without crude oil in the annular environment.

In addition, the water content of the corrosion medium changes with the service life of oil well [18,21]. Thus, the SCC behavioral mechanism of the casing changes because of the change of electrical conductivity of the medium. However, a comprehensive understanding of the effect of these factors on the corrosion behavior of tubing in oil wells is lacking.

Designers of oil field generally use two methods for tubing material selection: (1) Select the material according to the mechanical strength of the tubing and completely ignore the stress corrosion cracking (SCC) of the oil well [22]; (2) Select materials according to the working condition of the oil well annulus and NACE TM0177 standard (a test standard for SCC resistance of pressure vessel materials in acidic sulfide environment without considering the inhibition effect of oil film) [23]. However, these methods cannot meet the demand of the oil field [24–26]. Therefore, a comprehensive investigation into the corrosion behavior of tubing in the annulus environment of oil fields, as well as the analysis of the mechanism of SCC and the gaining of control of corrosion are necessary, all of which can provide a reference for material selection and prevention.

In this study, the SCC behavior of L80 casing steel was studied by simulating the annulus environment of production wells using the electrochemical measurement method, immersion test, and tensile test under high temperature and high pressure. The effects of partial pressure of CO_2 (P_{CO_2}), partial pressure of H_2S (P_{H_2S}), water content, and different preloading stresses were studied to fully understand the SCC behavior of L80 steel.

2. Experimental

2.1. Material and Medium

Specimens were obtained from L80 casing steel. The chemical composition of L80 casing steel is listed in Table 1. The microstructure of casing steels is shown in Figure 1, and the mechanical performance is listed in Table 2. The metallographic sample of L80 steel (Length × Width × Height: 10 mm × 10 mm × 2 mm) was ground using sandpaper of up to #2000 grit. Then, the sample was polished with 0.5 µm diamond paste. Finally, the sample was etched by 4% (volume) nital and observed under metallurgical microscope (VHX-2000, Keyence, Japan). L80 steel was made of tempered sorbite.

Table 1. Chemical composition of casing steels (unit: wt%).

Steel	C	Si	Mn	*P*	S	Cr	Cu	Fe
L80	0.29	0.24	1.52	0.010	0.0033	<0.10	0.028	Bal.

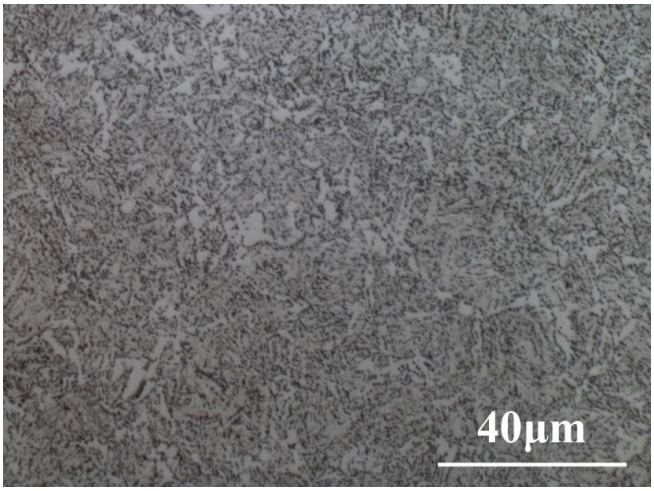

Figure 1. Microstructure of L80 steel.

Table 2. Mechanical performance of L80 steel used in this study.

Steel	Yield Strength R_{eL} (MPa)	Tensile Strength R_m (MPa)	Elongation δ_0 (%)	Reduction of Area ψ (%)
L80	633	731	24.8	74.6

According to the analysis of an oil field, the test medium was an oil–water mixture, which was composed of mineralized water and crude oil, the composition of mineralized water was as follows: 236.5 $g \cdot L^{-1}$ of NaCl, 1.01 $g \cdot L^{-1}$ of $NaHCO_3$, 0.64 $g \cdot L^{-1}$ of Na_2SO_4, 26.64 $g \cdot L^{-1}$ of $CaCl_2$, 12.68 $g \cdot L^{-1}$ of $MgCl_2 \cdot 6H_2O$. The pH of mineralized water was 6.

The water content of the produced medium of oil field was related to the service time of oil well [18]. The proportion of mineralized water (water content) in the test medium was set as 5 wt%, 30 wt%, 50 wt%, 80 wt%, and 100 wt% to simulate the produced medium of an oil field with different service times.

2.2. Potentiodynamic Polarization Measurement

Under the service condition of oil casing, the P_{CO_2}, P_{H_2S}, and water content of corrosive medium affected the electrochemical corrosion behavior of oil casing. Therefore, potentiodynamic polarization measurement was used to evaluate the effects of the abovementioned factors on corrosion behavior. The potentiodynamic polarization curves were measured under different conditions (as shown in Table 3) by using a three-electrode system in the autoclave. The L80 steel was used as the research electrode, Ag/AgCl electrode as the reference electrode, and platinum plate electrode as the auxiliary electrode. The size of the electrochemical test sample was 10 mm × 10 mm × 4 mm. After welding with copper wire, the L80 steel was sealed with epoxy resin, and the exposed area was 1 cm^2. The exposed surface of specimens was ground using sandpaper of up to #2000 grit. Then, the specimens were rinsed with ethanol, degreased with acetone, and dried with compressed air. The test temperature was set at 80 °C. The scanning rate of the potentiodynamic polarization test was 0.5 mV s^{-1}, and the scanning potential ranged from −0.4 V to 0.7 V (vs. OCP). Before the test, the experimental medium was deoxidized by high-purity nitrogen for 2 h, and the research electrode was polished using 2000-grit sandpapers. After degreasing using acetone, the research electrode was dried for standby. During data processing, all the measured potential were converted into another potential, which refers to the saturated calomel electrode.

Table 3. Test conditions of polarization measurement.

Experiment	P_{CO_2} (MPa)	P_{H_2S} (MPa)	Water Content (%)	Temperature (°C)
1-1	0	0.15	80	80
1-2	0.5			
1-3	1.1			
1-4	1.25			
2-1	1.1	0	80	80
2-2		0.03		
2-3		0.06		
2-4		0.15		
2-5		0.3		
3-1	1.1	0.15	30	80
3-2			50	
3-3			80	
3-4			100	

2.3. Immersion Test

Immersion test was conducted under different conditions (as shown in Table 4). Before the test, specimens were cleaned, dried, and weighed. Then, specimens and test

medium were added into the autoclave. Next, the test medium was deoxygenated by purging nitrogen for 2 h. Finally, different experimental conditions were applied, and the immersion test began. All immersion tests lasted for 720 h, and the test temperature was set at 80 °C.

Table 4. Test conditions of immersion test.

Experiment	P_{CO_2} MPa	P_{H_2S} MPa	Water Content %	Temperature °C	Preloading Stress (R_{eL})
4-1	0.5				
4-2	1.1	0.15	80	80	0
4-3	1.5				
5-1		0.03			
5-2	1.1	0.15	80	80	0
5-3		0.3			
6-1			30		
6-2	1.1	0.15	50	80	0
6-3			80		
6-4			100		
7-1					0.5
7-2	1.1	0.15	80	80	0.8
7-3					1.0

After immersion, all specimens were cleaned, dried, and weighed again. The corrosion rate of specimens was calculated by Equation (1): [27,28]

$$v_d = \frac{w_0 - w_1}{\rho \cdot S \cdot t} \times 8,760,000 \quad (1)$$

where v_d is the corrosion rate, mm y^{-1}; w_0 is the weight of the specimen before immersion, g; w_1 is the weight of the specimen after immersion, g; ρ is the density of the steel, which is 7.86 g cm^{-3}; S is the superficial area of the specimen before immersion, mm^2; t is the time spent by the immersion test, h. All tests were repeated three times for reliable results.

2.4. Slow Strain Rate Test (SSRT) after Immersion

Tensile tests were conducted on other parallel immersed specimens according to ASTM E8M-09 [29]. The size of the tensile specimens is shown in Figure 2. Before the tensile test, the tensile specimens were immersed for 720 h under different conditions (as shown in Table 4). All tensile tests were conducted with a CORTEST slow strain rate test system (CORTEST, Willoughby, OH, USA). The test system can control temperature and gas pressure during tensile test. The tensile rate was 10^{-6} s^{-1}. Then, elongations and reductions in the area were obtained from the stress–strain curves. Furthermore, the SCC susceptibility of the L80 steel was calculated by Equations (2)–(4): [30–32]

$$I_\delta = (1 - \frac{\delta_s}{\delta_0}) \times 100\% \quad (2)$$

$$I_\psi = (1 - \frac{\psi_s}{\psi_0}) \times 100\% \quad (3)$$

$$I_{R_m} = (1 - \frac{R_{ms}}{R_{m0}}) \times 100\% \quad (4)$$

where I_δ, I_ψ, and I_{Rm} are the susceptibilities of SCC calculated by different parameters; δ, ψ, and R_m are the elongations, reduction of area, and tensile strength, respectively; subscript s and subscript 0 represent the parameters of steel in corrosion medium and air, respectively. All tests were repeated three times for reliable results.

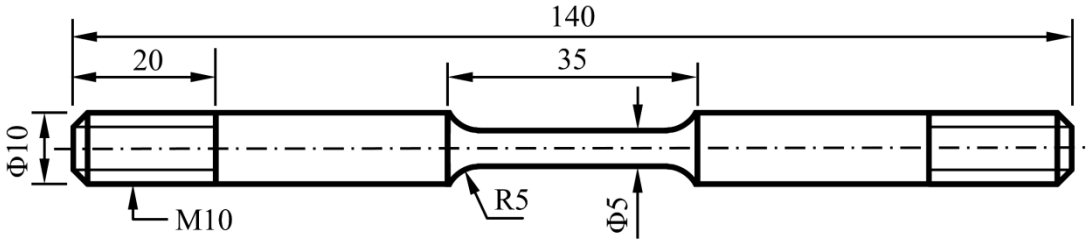

Figure 2. Size of the tensile specimen (unit: mm).

3. Results

3.1. Corrosion Behavior of L80 Steel without Preloading Stress

3.1.1. Effect of Environmental Factors on the Electrochemical Behavior of L80 Steel without Preloading Stress

Firstly, the effect of temperature on electrochemical corrosion behavior is studied using polarization curves, as shown in Figure 3. It can be found that the corrosion potential of L80 steel shifts negatively as the temperature increases. However, the corrosion current density of L80 steel reaches a maximum at 80 °C. Therefore, 80 °C was chosen to research the effect of other factors on the corrosion behavior of L80 steel.

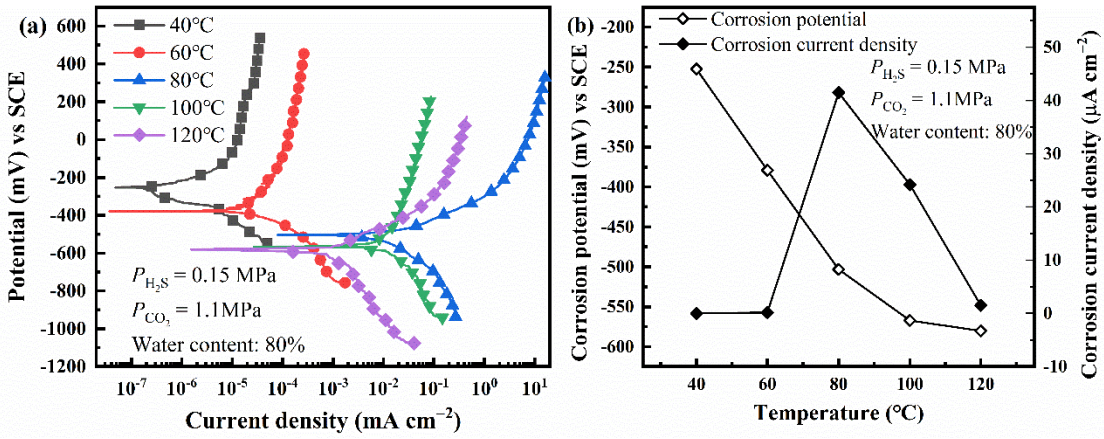

Figure 3. Polarization curves (**a**) and fitting results (**b**) of L80 steels under different temperature.

The polarization curves of L80 steel under different experimental conditions are shown in Figure 4a,c,e. Figure 4b,d,f shows the variation of corrosion potential and corrosion current density with different factors, which is obtained by fitting polarization curves. The environmental factors (P_{CO_2}, P_{H_2S}, and water content) can affect the polarization behavior of L80 steel. However, when a single factor changes, all the curves have the same shape, which indicates that the variation of a single factor does not affect the corrosion mechanism of L80 steels and the rate-controlling step of corrosion (electrochemical reaction step).

As P_{CO_2} increases, the corrosion potential of L80 steel shifts positively; meanwhile, the corrosion current density increases initially and then decreases. The partial pressure related to the largest corrosion current density is called critical pressure, which is 1.1 MPa. The effect of P_{CO_2} on corrosion potential and corrosion current density is partially attributed to the change of pH caused by the solution of CO_2 in the corrosion medium [1,4].

As the partial pressure of H_2S increases, the corrosion potential of L80 steel shifts negatively first and then shifts positively. In addition, the corrosion current density decreases initially and then increases. Therefore, the increase of P_{H_2S} restrains the corrosion of L80 steel in the test medium when the P_{H_2S} is less than the critical pressure (0.06 MPa), which may be related to the competitive adsorption of CO_2 and H_2S on the surface of L80 steel [28,33].

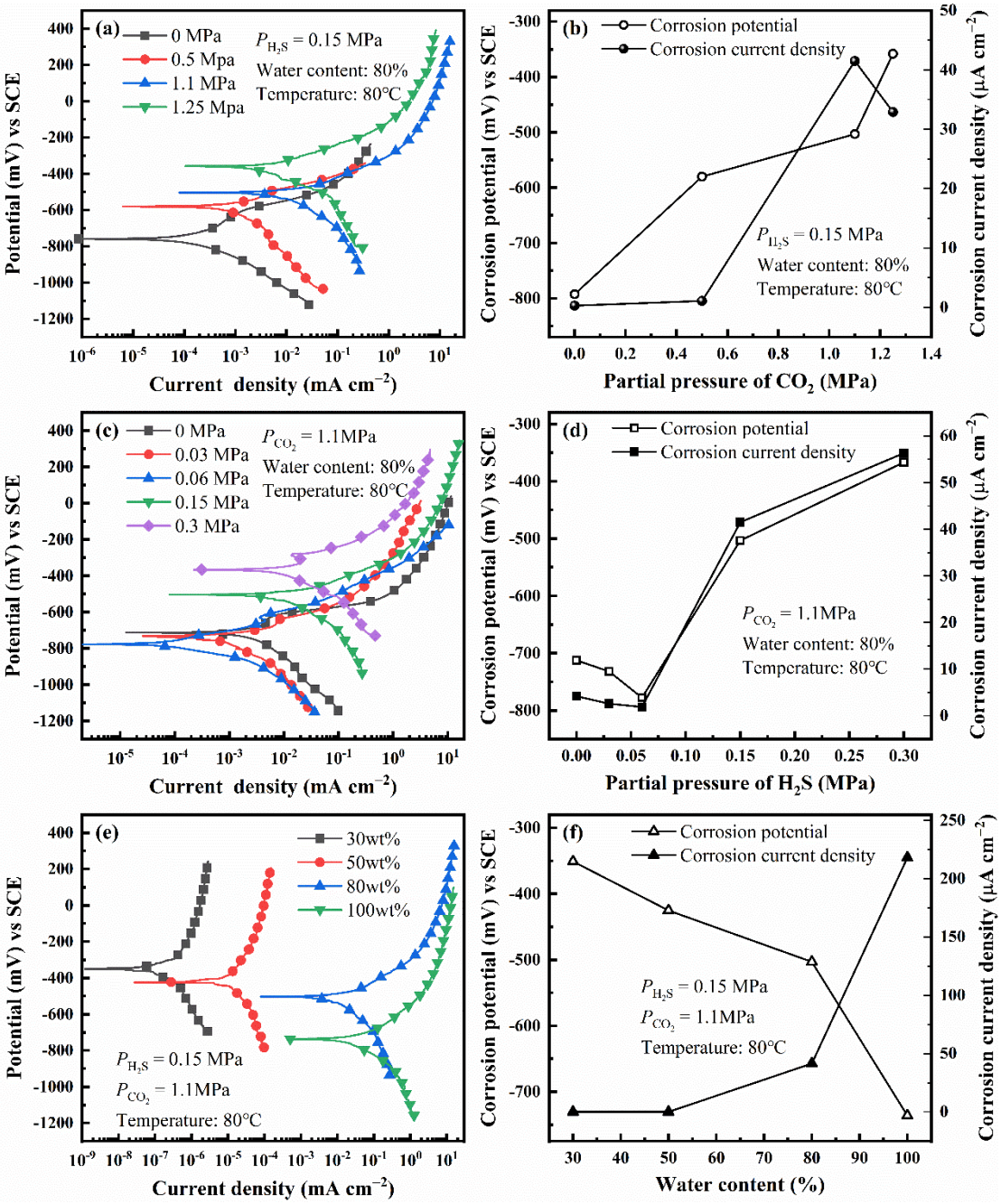

Figure 4. Polarization curves and fitting results of L80 steels under different partial pressure of CO_2 (**a**,**b**), different partial pressure of H_2S (**c**,**d**) and different water content (**e**,**f**).

When the water content changes, the corrosion potential of L80 steel shifts negatively, and the corrosion current density increases with water content. Comparing the four polarization curves under different water content, water content can promote the anodic and cathodic processes of corrosion simultaneously.

In verifying the results from the polarization curves, the L80 steel without preloading stress was immersed under different experimental conditions. The corrosion rate of L80 steel was calculated by Equation (1) (Figure 5).

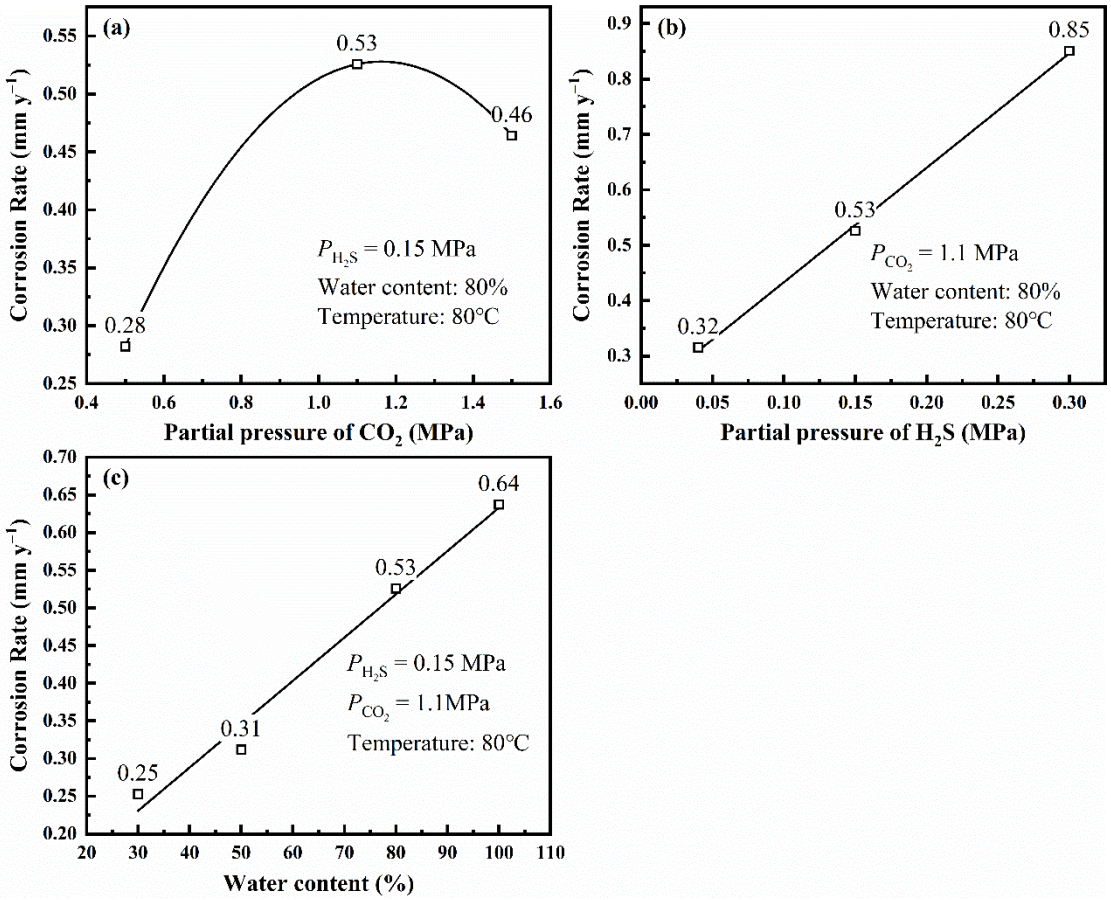

Figure 5. Corrosion rate of L80 steel without preloading stress obtained from immersion test under different partial pressure of CO_2 (**a**), different partial pressure of H_2S (**b**), and different water content (**c**).

The results from the immersion test are consistent with those from the polarization curves. When P_{CO_2} is 1.1 MPa, the L80 steel has the biggest corrosion rate. As P_{H_2S} (>0.15 MPa) and water content increase, the corrosion rate of L80 steel under experimental condition increases.

3.1.2. SCC Susceptibility of L80 Steel without Preloading Stress after Immersion

Based on the electrochemical behavior of L80 steel, the temperature was set at 80 °C. The P_{CO_2}, P_{H_2S}, and water content were changed to study their effect on the SCC susceptibility of L80 steel. Figure 6a,c,e shows the stress–strain curves of L80 steel under different conditions after the 720 h immersion of tensile samples in the test medium.

Figure 6b,d,f shows the variation of the SCC susceptibility of L80 steel with different P_{CO_2}, P_{H_2S}, and water content calculated by Equations (2)–(4). Yield strength (R_{eL}), tensile strength (R_m), and reduction of the area (ψ) change slightly as P_{CO_2}, P_{H_2S}, and water content increase. I_{Rm} and I_ψ are all less than 4%, the change of which is too small to reflect the change of the SCC susceptibility of L80 steel [18]. Moreover, I_δ is fitter for analyzing the change of the SCC susceptibility because of the evident change. The value of I_δ is shown in Table 5. The influence of P_{CO_2} on I_δ has an inflection point of approximately 1.1 MPa. The I_δ reaches the maximum when the P_{CO_2} is about 1.1 MPa. I_δ has a positive correlation to P_{H_2S} and water content.

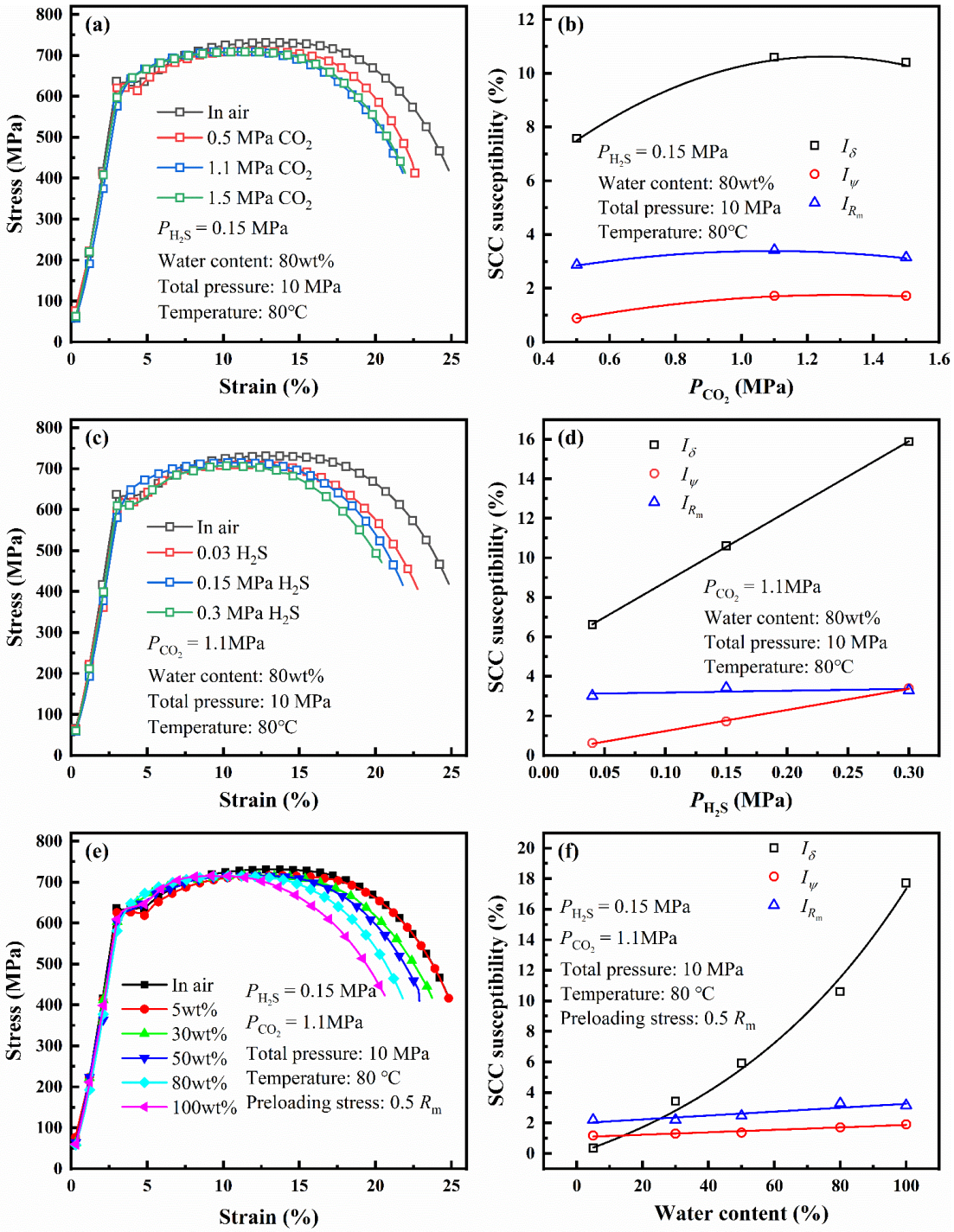

Figure 6. Stress–strain curves and SCC susceptibility of L80 steel under different partial pressure of CO_2 (**a**,**b**), different partial pressure of H_2S (**c**,**d**) and water content (**e**,**f**).

Table 5. The SCC susceptibility of L80 steel under different conditions.

Parameters	Numerical Value				
P_{CO_2} (MPa)	0.5	1.1	1.5		
I_δ (%)	7.58	10.60	10.40		
P_{H_2S} (MPa)	0.03	0.15	0.30		
I_δ (%)	6.61	10.60	15.88		
Water content (%)	5	30	50	80	100
I_δ (%)	0.36	3.42	5.93	10.60	17.73

When P_{CO_2} is higher than 1.1 MPa, the stress–strain curves and the SCC susceptibility of L80 steel change slightly, which indicates that P_{CO_2} slightly affects SCC of steel. However, the variation of the SCC susceptibility of L80 steel with different P_{H_2S} is larger than that with different P_{CO_2}. Therefore, the SCC of L80 in the test medium is more sensitive to H_2S than CO_2. Water content also has a great influence on the SCC susceptibility of L80 steel. The SCC susceptibility of L80 steel increases with the water content of the corrosion medium.

3.2. Corrosion Behavior of L80 Steel with Preloading Stress

After the downhole tubes are adjusted, the tubes must perform under environmental stress, which can affect the SCC behavior of tubes. Therefore, different levels of initial stress (preloading stress) are applied to the tensile specimen to study how preloading stress affects the corrosion behavior of L80 steel.

Figure 7 shows the corrosion rate (calculated by weight–loss method) of L80 steel with different preloading stresses after the 720 h immersion test. The corrosion rate of L80 steel under the experimental conditions increases with preloading stress. Preloading stress can promote the corrosion of L80 steel. The corrosion rate of L80 steel has a positive correlation to preloading stress.

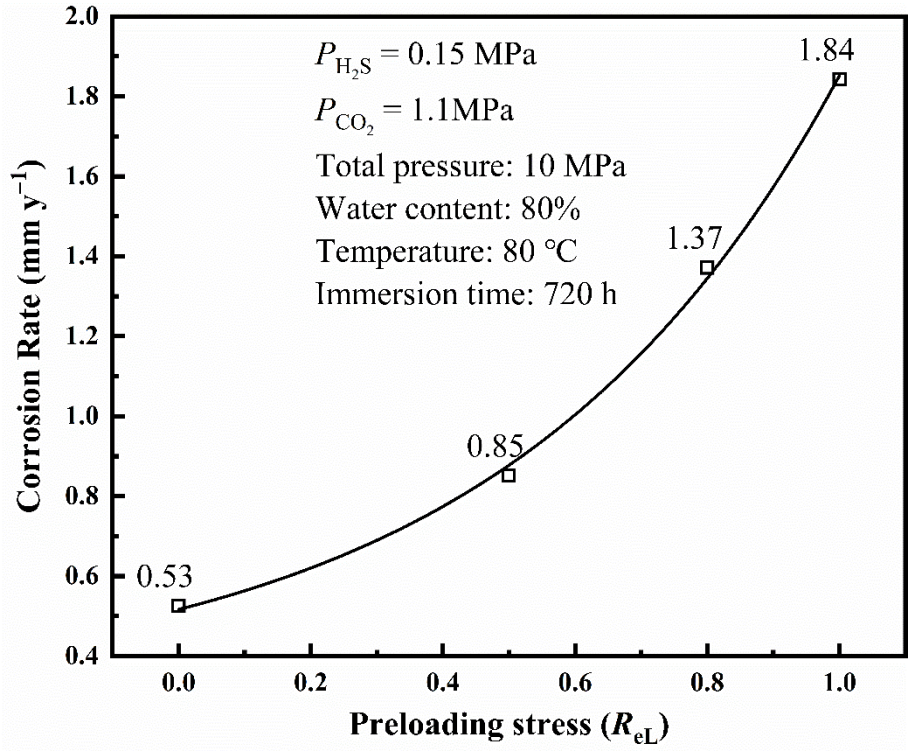

Figure 7. Corrosion rate of L80 steel with different preloading stresses obtained from immersion test.

Figure 8a shows the stress–strain curves of L80 steel under different preloading stresses after 720 h immersion. The SCC susceptibility of L80 was calculated using Equations (2)–(4)

(Figure 8b). The SCC susceptibility increases with preloading stress. Similarly, I_δ is a good parameter to evaluate SCC susceptibility compared with I_{Rm} and I_ψ. The value of I_δ is shown in Table 6. I_δ also has a positive correlation to preloading stress, which is similar to the relation between corrosion rate and preloading stress.

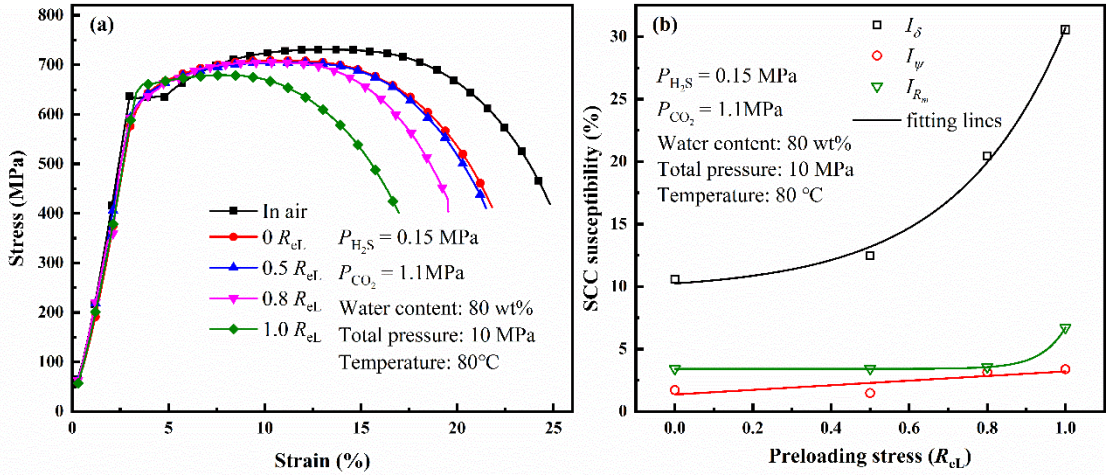

Figure 8. Stress–strain curves of L80 steel with different preloading stresses (**a**) and variation of the SCC susceptibility of L80 steel with different preloading stresses (**b**).

Table 6. The SCC susceptibility of L80 steel under different preloading stress.

Parameters	Numerical Value			
Preloading stress (R_{eL})	0	0.5	0.8	1.0
I_δ (%)	10.60	12.45	20.48	30.55

4. Discussion

When downhole tubes service in a CO_2/H_2S environment, the corrosion behavior of tubes is affected by P_{CO_2} and P_{H_2S}, which is complex. After CO_2 dissociates into the corrosion medium containing water, the following reactions occur: [34,35]

$$CO_2 + H_2O \rightleftharpoons H_2CO_3 \quad (5)$$

$$H_2CO_3 \rightleftharpoons H^+ + HCO_3^- \quad (6)$$

$$HCO_3^- \rightleftharpoons H^+ + CO_3^{2-} \quad (7)$$

Carbonic acid (H_2CO_3) is a weak acid, which can serve as a buffer and keep the pH of the medium at a relatively low value because of the incomplete ionization of H_2CO_3 [35]. When H_2S appears in the solution, reactions similar to Equations (8) and (9) occur, which can also keep the solution acidic [28,36]. The acidic environment can accelerate the corrosion of casing steel. The anodic process is the dissolution of steel (Equation (10)), and the cathodic process is hydrogen evolution reaction (Equation (11)). Hydrogen atoms generated during hydrogen evolution reaction can increase the SCC susceptibility of tubular steels because hydrogen atoms can penetrate the steel substrate [37]. Therefore, every change that can promote hydrogen evolution reaction will increase the SCC susceptibility of tubular steels.

$$H_2S \rightleftharpoons HS^- + H^+ \quad (8)$$

$$HS^- \rightleftharpoons S^{2-} + H^+ \quad (9)$$

When P_{CO_2} increases from 0 MPa to 1.5 MPa, the pH of the solution decreases gradually, and the equilibrium potential of hydrogen evolution reaction shifts positively. The mixed potential of the corrosion system, corrosion potential, is the result of the coupling

of metal dissolution reaction and hydrogen evolution reaction. Therefore, the corrosion potential of steel in the corrosion medium increases with P_{CO_2} (Figure 4b) [4]. As P_{CO_2} changes from 0 MPa to 1.1 MPa, dwindling pH accelerates the corrosion of steel. The further increase of P_{CO_2} can increase the concentration of CO_3^{2-}; then, Ca^{2+}, Mg^{2+}, and Fe^{2+} interact with CO_3^{2-}, which forms insoluble carbonate precipitation (Equations (12)–(14)) [4,6]. Precipitation can cover the anode surface (where the concentration of Fe^{2+} is larger than that on the cathodic area), suppress the anodic reaction, and then decrease the corrosion rate of steel. Corrosion is the coupling of anodic and cathodic reactions [38]. Therefore, the hydrogen evolution reaction is also restricted. The less hydrogen formed on the surface of the steel, the lower the SCC susceptibility of steel [39]. Thus, the results of SSRT (Figure 6a,b) show that the L80 steel achieves the highest SCC susceptibility when P_{CO_2} is 1.1 MPa. Figure 3 shows that the corrosion current density of L80 steel reaches a maximum at 80 °C. This is because the higher temperature can improve the corrosion reaction activity and the precipitation of carbonate ($FeCO_3$ and $CaCO_3$) [40]. When the temperature is lower than 80 °C, the improvement in reaction activity dominates the corrosion process and the corrosion rate increases with temperature. When the temperature is higher than 80 °C, the effect of temperature on the precipitation of $FeCO_3$ and $CaCO_3$ dominates the corrosion process; the corrosion rate decreases with temperature.

$$Fe \rightarrow Fe^{2+} + 2e^- \quad (10)$$

$$H^+ + e^- \rightarrow H \quad (11)$$

$$Mg^{2+} + CO_3^{2-} \rightleftharpoons MgCO_3 \quad (12)$$

$$Ca^{2+} + CO_3^{2-} \rightleftharpoons CaCO_3 \quad (13)$$

$$Fe^{2+} + CO_3^{2-} \rightleftharpoons FeCO_3 \quad (14)$$

$$Fe^{2+} + S^{2-} \rightleftharpoons FeS \quad (15)$$

Under a CO_2/H_2S environment, the effect of P_{H_2S} on the corrosion of steel differs from that of P_{CO_2}. Some researchers have reported that the CO_2/H_2S ratio can affect the corrosion behavior of steel [4,6,33,41]. The corrosion product scale can be formed on the surface of steel as corrosion develops in a high-pressure CO_2/H_2S environment (Equations (12)–(15)) [42,43]. As P_{H_2S} increases, the corrosion of the L80 steel is under the mixed control of CO_2 and H_2S. The proportion of Fe_xS in the corrosion product film also increases [9].

In the corrosion medium, H_2S can inhibit the hydrolysis of CO_2, and the adsorption of H_2S competes with CO_2 [28]. Moreover, Fe^{2+} can easily interact with S^{2-} to form precipitation [40]. As the cathode, the precipitation (FeS) can promote the corrosion of L80 steel. When P_{H_2S} is less than 0.06 MPa, H_2S can restrain the corrosion of L80 steel. The corrosion potential shifts negatively, and the corrosion rate decreases. When P_{H_2S} is higher than 0.06 MPa, H_2S also has the abovementioned function (inhibiting the hydrolysis of CO_2, the adsorption of H_2S competes with CO_2, and promoting the precipitation of FeS). However, dissolving enough H_2S in the corrosion medium promotes hydrolysis and acidifies the medium, which can make up for the inhibited promoting effect of CO_2 on the cathode process [11]. Therefore, an increase in P_{H_2S} can increase the corrosion rate of steel and positively shift the corrosion potential.

Although the corrosion rate of L80 steel decreases and then increases as P_{H_2S} increases, the SCC susceptibility of L80 steel always increases as P_{H_2S} increases because H_2S is a poisoning agent, which can increase the hydrogen content in the interior of L80 steel [11]. Hydrogen in the interior of steel can promote stress corrosion.

The water content of the corrosion medium is also an important factor that affects the SCC of L80 steel. As water content increases, the electrical conductivity of the corrosion medium increases. High electrical conductivity can promote the corrosion of L80 steel. In addition, excessive hydrogen can diffuse into the steel and deteriorate the SCC resistance

of L80 steel. When the water content is relatively low, the electrical conductivity of the corrosion medium is low, and the corrosion of steel becomes restricted. Moreover, excessive oil can form an oil film on the surface of steel and separate the steel from the corrosion medium, which can also suppress the corrosion of L80 steel.

During the service period, not only the corrosion medium but also the environmental stress affects the corrosion behavior of the L80 steel. In this study, preloading is less than or equal to R_{eL}. The corrosion rate and SCC susceptibility of the L80 steel both have a positive correlation to preloading stress. When the steel is under an elastic stress state, the stress can lead to dislocation emergence, and a small number of dislocations start to produce defects [44]. These defects increase with the stress level. The dislocation emergence point is a high distortion area with high chemical activity, which can promote corrosion reactions. When stress is equal to R_{eL}, the dislocations begin to slip. Then, plastic deformation and many defects occur. These defects can also promote the corrosion of steel. Therefore, as the preloading stress changes from 0 R_{eL} to 1 R_{eL}, the number of defects increases rapidly, and the corrosion rate of the L80 steel increases. A higher corrosion rate can produce more adsorbed hydrogen atoms. Furthermore, the lattice distortion caused by tensile stress can improve the diffusion of hydrogen into steel. According to existing research [45–47], interstitial atoms (such as carbon atoms) can interact with dislocations and result in dislocation stacking during plastic deformation. However, hydrogen atoms in steel can promote dislocation emission and motion. Next, hydrogen could cause local stress concentration and initiate hydrogen-induced microcracks [48]. Therefore, more hydrogen can diffuse into the steel and promote the SCC of L80 steel.

P_{CO_2}, P_{H_2S}, water content, and preloading stress can affect the SCC behavior of L80 steel. A change in these factors can affect the corrosion of L80 steel and the rate of hydrogen evolution reaction. The faster the rate of hydrogen evolution reaction, the more hydrogen diffused into steel, and the higher the SCC susceptibility.

5. Conclusions

The results of this study suggest that service environmental parameters (P_{CO_2}, P_{H_2S}, water content, and preloading stress) can affect the electrochemical corrosion behavior of L80 steel.

(1) The P_{CO_2} affects the corrosion behavior of steel in two aspects: Keeping the pH of the medium at a relatively low value and promoting form insoluble carbonate precipitation. The influence of P_{CO_2} on the corrosion rate and SCC susceptibility has an inflection point of approximately 1.1 MPa. The corrosion rate and SCC susceptibility reached the maximum when the P_{CO_2} is about 1.1 MPa;

(2) The P_{H_2S} also affects the corrosion behavior of steel from two aspects: Inhibiting the hydrolysis of CO_2 and promoting formation of FeS precipitation. The corrosion rate and SCC susceptibility have a positive correlation to P_{H_2S};

(3) Corrosion rate has a linear relation to water content, and SCC susceptibility has a positive correlation to water content. Low water content can decrease the electrical conductivity of the corrosion medium and then restrict the corrosion of L80 steel;

(4) The corrosion rate and SCC susceptibility of L80 steel have a positive correlation to preloading stress. SCC susceptibility of L80 steel can be explained by the local additional potential model. It means that preloading stress can promote the occurrence of defects in the surface of L80 steel. These defects can facilitate local corrosion, accelerate the diffusion of hydrogen into steel, and then increase SCC susceptibility.

Author Contributions: Conceptualization, Z.L. (Zhiyong Liu) and L.L.; methodology, X.S., H.C. and Z.L. (Zhiyong Liu); validation, X.S., H.C., Z.L. (Zhong Li), R.H. and Z.L. (Zhiyong Liu); formal analysis, X.S.; investigation, X.S., H.C., Z.L. (Zhong Li), Z.L. (Zhiyong Liu) and L.L.; resources, Z.L. (Zhiyong Liu); data curation, X.S.; writing—original draft preparation, X.S.; writing—review and editing, X.S., H.C., Z.L. (Zhong Li), Z.L. (Zhiyong Liu) and L.L.; visualization, X.S.,

H.C., Z.L. (Zhong Li) and R.H.; supervision, Z.L. (Zhiyong Liu) and L.L.; funding acquisition, Z.L. (Zhiyong Liu). All authors have read and agreed to the published version of the manuscript.

Funding: This work was financially supported by Fundamental Research Funds for the Central Universities (No. FRF-NP-20-04).

Institutional Review Board Statement: Not applicable.

Informed Consent Statement: Not applicable.

Data Availability Statement: Not applicable.

Conflicts of Interest: The authors declare no conflict of interest.

References

1. Gao, X.; Zhang, D.; Lu, Y.; Fan, Z.; Du, L.; Yuan, G.; Qiu, C.; Kang, J. CO_2 Corrosion Behavior of High-Strength and Toughness V140 Steel for Oil Country Tubular Goods. *J. Mater. Eng. Perform.* **2020**, *29*, 8451–8460. [CrossRef]
2. Sun, C.; Zeng, H.; Luo, J.-L. Unraveling the Effects of CO_2 and H_2S on the Corrosion Behavior of Electroless Ni-P Coating in $CO_2/H_2S/Cl^-$ Environments at High Temperature and High Pressure. *Corros. Sci.* **2019**, *148*, 317–330. [CrossRef]
3. Abayarathna, D.; Naraghi, A.R.; Wang, S. *The Effect of Surface Films on Corrosion of Carbon Steel in a CO_2-H_2S-H_2O System*; NACE International: Houston, TX, USA, 2005.
4. Cui, H.; Mei, P.; Liu, Z.; Lu, L. Effect of CO_2 Partial Pressure on the Stress Corrosion Cracking Behavior of N80 Tubing Steel in the Annulus Environment of CO_2 Injection Well. *Chin. J. Eng.* **2020**, *42*, 1182–1189.
5. Zhang, C. Study of the Corrosion Inhibition Mechanism and the Synergistic Corrosion Inhibition Effect of Inhibitors CO_2/H_2S System. Master's Thesis, Beijing University of Chemical Technology, Beijing, China, 2018.
6. Liu, Z.Y.; Wang, X.Z.; Liu, R.K.; Du, C.W.; Li, X.G. Electrochemical and Sulfide Stress Corrosion Cracking Behaviors of Tubing Steels in a H_2S/CO_2 Annular Environment. *J. Mater. Eng. Perform.* **2014**, *23*, 1279–1287. [CrossRef]
7. Parkins, R.N.; Zhou, S. The Stress Corrosion Cracking of C-Mn Steel in CO_2-HCO_3^--CO_3^{2-} Solutions. I: Stress Corrosion Data. *Corros. Sci.* **1997**, *39*, 159–173. [CrossRef]
8. Zhou, C.; Zheng, S.; Chen, C.; Lu, G. The Effect of the Partial Pressure of H_2S on the Permeation of Hydrogen in Low Carbon Pipeline Steel. *Corros. Sci.* **2013**, *67*, 184–192. [CrossRef]
9. Monnot, M.; Nogueira, R.P.; Roche, V.; Berthomé, G.; Chauveau, E.; Estevez, R.; Mantel, M. Sulfide Stress Corrosion Study of a Super Martensitic Stainless Steel in H_2S Sour Environments: Metallic Sulfides Formation and Hydrogen Embrittlement. *Appl. Surf. Sci.* **2017**, *394*, 132–141. [CrossRef]
10. Zhou, C.; Huang, Q.; Guo, Q.; Zheng, J.; Chen, X.; Zhu, J.; Zhang, L. Sulphide Stress Cracking Behaviour of the Dissimilar Metal Welded Joint of X60 Pipeline Steel and Inconel 625 Alloy. *Corros. Sci.* **2016**, *110*, 242–252. [CrossRef]
11. Jia, Y. *Study on Stress Corrosion Sensitivity of Cold Deformed 316L Austenitic Stainless Steel in H_2S Environment*; China University of Petroleum: Beijing, China, 2019.
12. Wang, S. *Multiphysical Simulation of CO_2 Enhanced Oil Recovery in Unconventional Reservoirs: From Fundamental Physics to Simulator Development*; Colorado School of Mines: Golden, CO, USA, 2019.
13. Liu, Q.; Li, Z.; Liu, Z.Y.; Li, X.G.; Wang, S.Q. Effects of H_2S/HS^- on Stress Corrosion Cracking Behavior of X100 Pipeline Steel Under Simulated Sulfate-Reducing Bacteria Metabolite Conditions. *J. Mater. Eng. Perform.* **2017**, *26*, 2763–2775. [CrossRef]
14. Vyboishchik, M.A.; Ioffe, A.V.; Zyryanov, A.O. Failure of Pump–Compressor Pipes in Highly Aggressive Oil-Field Media. *Russ. Metall.* **2019**, *2019*, 1067–1073. [CrossRef]
15. Khalaf, A.M.; Seibi, A.C. Failure Analysis of Lube Oil Feed Tube of a Gas Turbine Operating in Oil Fields. *Eng. Fail. Anal.* **2011**, *18*, 1341–1350. [CrossRef]
16. De Assis Severiano, J.; Silva, A.S.; Sussushi, E.M.; da Silva Sant'Anna, M.V.; da Cunha, M.A.; Bergmann, C.P.; Griza, S. Corrosion Damages of Flow Regulation Valves for Water Injection in Oil Fields. *Eng. Fail. Anal.* **2019**, *96*, 362–373. [CrossRef]
17. Liu, R.; Li, J.; Liu, Z.; Du, C.; Dong, C.; Li, X. Effect of PH and H_2S Concentration on Sulfide Stress Corrosion Cracking (SSCC) of API 2205 Duplex Stainless Steel. *IJMR* **2015**, *106*, 608–613. [CrossRef]
18. Zhao, T.; Liu, Z.; Du, C.; Hu, J.; Li, X. A Modelling Study for Predicting Life of Downhole Tubes Considering Service Environmental Parameters and Stress. *Materials* **2016**, *9*, 741. [CrossRef] [PubMed]
19. Yucheng, L.; Yinlong, Z.; Jianmei, Y.; Mengjing, Y.; Junzhong, X. Research on Corrosion Perforation on Pipeline by Media of High Salinity Acidic Oil–Water Mixture. *Eng. Fail. Anal.* **2013**, *34*, 35–40. [CrossRef]
20. Bouazaze, H.; Huet, F.; Nogueira, R.P. A New Approach for Monitoring Corrosion and Flow Characteristics in Oil/Brine Mixtures. *Electrochim. Acta* **2005**, *50*, 2081–2090. [CrossRef]
21. Liu, R. Stress Corrosion Cracking Behaviour and Prevention of High Strength Tubing Steels in Typical H_2S/CO_2 Annulus Environments. Ph.D. Thesis, University of Science and Technology Beijing, Beijing, China, 2015.
22. Hong, C.; Estefen, S.F.; Wang, Y.; Lourenço, M.I. Mixed-Integer Nonlinear Programming Model for Layout Design of Subsea Satellite Well System in Deep Water Oil Field. *Autom. Constr.* **2021**, *123*, 103524. [CrossRef]

23. *NACE International Standard: TM0177-2005 Laboratory Testing of Metals for Resistance to Sulfide Stress Cracking and Stress Corrosion Cracking in H2S Environments*; NACE International: Houston, TX, USA, 2005.
24. Li, N.; Ding, N.; Liu, L.; Hu, S.; Sun, S.; Qu, S.; Wu, C.-M.L. Stress Corrosion Cracking of an Electrohydraulic Oil Pipe. *J. Fail. Anal. Prev.* **2019**, *19*, 29–35. [CrossRef]
25. Wang, H.; Zhao, W.; Shu, Z.; Zhao, Q.; Han, L. Failure Analysis of Casing Dropping in Shale Oil Well During Large Scale Volume Fracturing. *Eng. Fail. Anal.* **2020**, *118*, 104849. [CrossRef]
26. Tian, J.; Wang, L.; Sun, W.; Yang, Y.; Liu, Z.; Wang, G.; Zhao, L.; Zhou, Y.; Liu, G. Failure Analysis of Steam Jet Pump at Top of Crude Oil Vacuum Distillation Tower. *Eng. Fail. Anal.* **2019**, *103*, 9–19. [CrossRef]
27. Liu, H.; Gu, T.; Zhang, G.; Wang, W.; Dong, S.; Cheng, Y.; Liu, H. Corrosion Inhibition of Carbon Steel in CO_2-Containing Oilfield Produced Water in the Presence of Iron-Oxidizing Bacteria and Inhibitors. *Corros. Sci.* **2016**, *105*, 149–160. [CrossRef]
28. Zhang, G.A.; Zeng, Y.; Guo, X.P.; Jiang, F.; Shi, D.Y.; Chen, Z.Y. Electrochemical Corrosion Behavior of Carbon Steel under Dynamic High Pressure H_2S/CO_2 Environment. *Corros. Sci.* **2012**, *65*, 37–47. [CrossRef]
29. American Society for Testing and Materials. Standard Test Method for Tension Testing of Metallic Materials. In *Annual Book of ASTM Standards*; ASTM International: West Conshohocken, PA, USA, 2014.
30. Wu, W.; Hao, W.; Liu, Z.; Li, X.; Du, C. Comparative Study of The Stress Corrosion Behavior of a Multiuse Bainite Steel in the Simulated Tropical Marine Atmosphere and Seawater Environments. *Constr. Build. Mater.* **2020**, *239*, 117903. [CrossRef]
31. Liu, Z.Y.; Hao, W.K.; Wu, W.; Luo, H.; Li, X.G. Fundamental Investigation of Stress Corrosion Cracking of E690 Steel in Simulated Marine Thin Electrolyte Layer. *Corros. Sci.* **2019**, *148*, 388–396. [CrossRef]
32. Wu, W.; Cheng, X.; Zhao, J.; Li, X. Benefit of The Corrosion Product Film Formed on a New Weathering Steel Containing 3% Nickel under Marine Atmosphere in Maldives. *Corros. Sci.* **2020**, *165*, 108416. [CrossRef]
33. Zheng, Y.; Ning, J.; Brown, B.; Nešić, S. Electrochemical Model of Mild Steel Corrosion in a Mixed H_2S/CO_2 Aqueous Environment in the Absence of Protective Corrosion Product Layers. *Corrosion* **2014**, *71*, 316–325. [CrossRef]
34. Barker, R.; Burkle, D.; Charpentier, T.; Thompson, H.; Neville, A. A Review of Iron Carbonate ($FeCO_3$) Formation in the Oil and Gas Industry. *Corros. Sci.* **2018**, *142*, 312–341. [CrossRef]
35. Cui, G.; Yang, Z.; Liu, J.; Li, Z. A Comprehensive Review of Metal Corrosion in a Supercritical CO_2 Environment. *Int. J. Greenh. Gas Control* **2019**, *90*, 102814. [CrossRef]
36. Li, Z.; Xu, X.; Li, Y.; Liu, Z. Effect of Imidazoline Inhibitor on Stress Corrosion Cracking of P110 Steel in Simulated Annulus Environments of CO2 Injection Well. *J. Electroanal. Chem.* **2021**, *886*, 115105. [CrossRef]
37. Li, Y.; Liu, Z.; Ke, L.; Huang, L.; Du, C.; Li, X. Stress Corrosion Cracking Behavior of TP95S Tube Steel in an Acidic Gas Field Environment. *Int. J. Electrochem. Sci.* **2016**, 5021–5034. [CrossRef]
38. Cao, C. *Principles of Electrochemistry of Corrosion*, 3rd ed.; Chemical Industry Press: Beijing, China, 2008.
39. Chen, Z.; Li, L.; Zhang, G.; Qiu, Y.; Guo, X. Inhibition Effect of Propargyl Alcohol on the Stress Corrosion Cracking of Super 13Cr Steel in a Completion Fluid. *Corros. Sci.* **2013**, *69*, 205–210. [CrossRef]
40. Haynes, W.M. *CRC Handbook of Chemistry and Physics*, 94th ed.; CRC Press: Boca Raton, FL, USA, 2013.
41. Liu, R.; Yin, G.; Wei, C.; Wang, X.; Ma, F.; Liu, Z.; Du, C.; Li, X. Electrochemical Corrosion Behaviour of P110 Tubing Steel in Annular Environment. *Corros. Sci. Prot. Technol.* **2013**, *25*, 450–454.
42. Zhao, X.; Huang, W.; Li, G.; Feng, Y.; Zhang, J. Effect of CO_2/H_2S and Applied Stress on Corrosion Behavior of 15Cr Tubing in Oil Field Environment. *Metals* **2020**, *10*, 409. [CrossRef]
43. Wang, Q.; Wu, W.; Li, Q. Under-Deposit Corrosion of Tubing Served for Injection and Production Wells of CO_2 Flooding. *Eng. Fail. Anal.* **2021**, *127*, 105540. [CrossRef]
44. Liu, Z.Y.; Li, X.G.; Du, C.W.; Cheng, Y.F. Local Additional Potential Model for Effect of Strain Rate on SCC of Pipeline Steel in an Acidic Soil Solution. *Corros. Sci.* **2009**, *51*, 2863–2871. [CrossRef]
45. Brechtl, J.; Chen, B.; Xie, X.; Ren, Y.; Venable, J.D.; Liaw, P.K.; Zinkle, S.J. Entropy Modeling on Serrated Flows in Carburized Steels. *Mater. Sci. Eng. A* **2019**, *753*, 135–145. [CrossRef]
46. Jiang, Z.; Zhu, L.; Yu, L.; Sun, B.; Cao, Y.; Zhao, Y.; Zhang, Y. The Mechanism for the Serrated Flow Induced by Suzuki Segregation in a Ni Alloy. *Mater. Sci. Eng. A* **2021**, *820*, 141575. [CrossRef]
47. Zhang, Y.; Liu, J.P.; Chen, S.Y.; Xie, X.; Liaw, P.K.; Dahmen, K.A.; Qiao, J.W.; Wang, Y.L. Serration and Noise Behaviors in Materials. *Prog. Mater. Sci.* **2017**, *90*, 358–460. [CrossRef]
48. Song, L.; Liu, Z.; Li, X.; Du, C. Characteristics of Hydrogen Embrittlement in High-PH Stress Corrosion Cracking of X100 Pipeline Steel in Carbonate/Bicarbonate Solution. *Constr. Build. Mater.* **2020**, *263*, 120124. [CrossRef]